AFRL-SR-BL-TR-00-

REPORT DOCUMENTATION PAGE

0142

1. AGENCY USE ONLY (Leave blank)	2. REPORT DATE	3. REPORT TYPE AND DATES COVERED
	3-Mar-00	Final Report: Nov 1, 1997 - October 31, 1999

4. TITLE AND SUBTITLE	5. FUNDING NUMBERS
High Speed Modulation, Beam Steering and Control of High Power Diode Lasers	F49620-97-1-0002

6. AUTHOR(S)
J. V. Moloney

7. PERFORMING ORGANIZATION NAME(S) AND ADDRESS(ES)
Department of Mathematics
University of Arizona
Tucson, Arizona 85721

8. PERFORMING ORGANIZATION REPORT NUMBER
Final Report FRS 301590

9. SPONSORING /MONITORING AGENCY NAMES(S) AND ADDRESS(ES)
AFOSR/PLK
110 Duncan Avenue Rm B115
Bolling AFB, DC 20332-8050

10. SPONSORING/MONITORING AGENCY REPORT NUMBER

11. SUPPLEMENTARY NOTES

12a. DISTRIBUTION/AVAILABILITY STATEMENT
Approved for public release; distribution unlimited.

12b. DISTRIBUTION CODE

13. ABSTRACT (Maximum 200 words)

This contract funded a major effort in bringing to maturity, a first-principles theory of semiconductor lasers and amplifiers based on a fully microscopic description of the light semiconductor material coupling. Signficant breakthroughs were made at the microscopic physics level by explicitly including all of the relevant excited bands in the active region of the device and obtaining quantitative agreement with gain/index and linewidth enhancement spectra measured for a variety of Quantum Well structures at the Air Force Research Laboratory, Albuquerque, NM. The full nonlinear pde model for high power wide aperture semiconductor lasers was reformulated theoretically so as to take advantage of speed and excellent parallel scaling of our ONYS2 in-house supercomputer. Resulting from this is the first interactive simulator for designing new generations of high brightness semiconductor devices. We were able to begin building a fully interactive platform-independent optoelectronic simulator which should have a major impact on designing sophisticated telecoms systems. Funding also allows major inroads in explaining the novel creation of an optically turbulent atmospheric light guide.

14. SUBJECT TERMS	15. NUMBER OF PAGES
	4
	16. PRICE CODE

17. SECURITY CLASSIFICATION OF REPORT	18. SECURITY CLASSIFICATION	19. SECURITY CLASSIFICATION OF ABSTRACT	20. LIMITATION OF ABSTRA
UNCLASSIFIED	UNCLASSIFIED	UNCLASSIFIED	UL

Final Report
November 1 1997 to October 31, 1999
F49620-97-1-0002
High Speed Modulation, Beam Steering and Control of High Power Diode Lasers

Arizona Center for Mathematical Sciences
Department of Mathematics
University of Arizona
PI: J.V. Moloney

Abstract

This contract funded a major effort in bringing to maturity, a first-principles theory of semiconductor lasers and amplifiers based on a fully microscopic description of the light semiconductor material coupling. Significant breakthroughs were made at the microscopic physics level by explicitly including all of the relevant excited bands in the active region of the device and obtaining quantitative agreement with gain/index and linewidth enhancement spectra measured for a variety of Quantum Well structures at the Air Force Research Laboratory, Albuquerque, New Mexico. The full nonlinear pde model for high power wide aperture semiconductor lasers was reformulated theoretically so as to take advantage of speed and excellent parallel scaling of our ONYX2 in-house supercomputer. Resulting from this is the first interactive simulator for designing new generations of high brightness semiconductor devices. We were able to begin building a fully interactive platform-independent optoelectronic simulator which should have a major impact on designing sophisticated telecoms systems. Contract funding also allowed us to make major inroads in explaining the novel creation of an optically turbulent atmospheric light guide. Again our excellent supercomputing resources provided by DURIP awards allowed us to build the sophisticated parallel solvers needed to resolve extremely sharp gradients associated with explosive intensity bursts and plasma generation.

Bandstructure and Microscopic Many-Body Gain Calculations

Significant progress was made in this task which allowed us to include all of the relevant valence and conduction bands occupied at high carrier densities both within the QW(s) and the confining barrier regions. Inclusion of the barrier states was essential to achieve convergence in the computation of the linewidth enhancement factor (LWEF), a quantity which is the ratio of the differential index to the differential gain. This quantity is therefore an extremely sensitive test of the reliability of the microscopic many-body theory unlike the gain lineshape which typically has converged on inclusion of the confined QW states only. A series of experiments carried out by D. Bossert at the Air Force Research Laboratory in Albuquerque, on the measurement of gain, index and LWEF spectra at different carrier densities provided a testbed for the theory. Structures with different QW widths and different SCH barrier widths were grown and the above quantities measured. Results from the theory-experiment comparisons are shown in the accompanying figure. The top picture is a schematic of a single InGaAs QW with a narrow Ga As SCH and an AlGaAs GRINSCH barrier. All of the conduction and valence band states included in the combined bandstructure/many-body calculation are shown in the top picture. The middle picture compares experimental (blue dots) and theoretical gain lineshapes at different carrier densities. The bottom picture contrasts the carrier density dependence of the LWEF for a 5 nm InGaAs and a 10 nm InGaAs QW. The LWEF for the narrow well clamps with increasing carrier density whereas it shows a linear increase with carrier density for the wider QW. As high power semiconductor laser diodes display strong nonuniformity of carrier density within the device, we expect to see a significantly different behavior for both types of active layer.

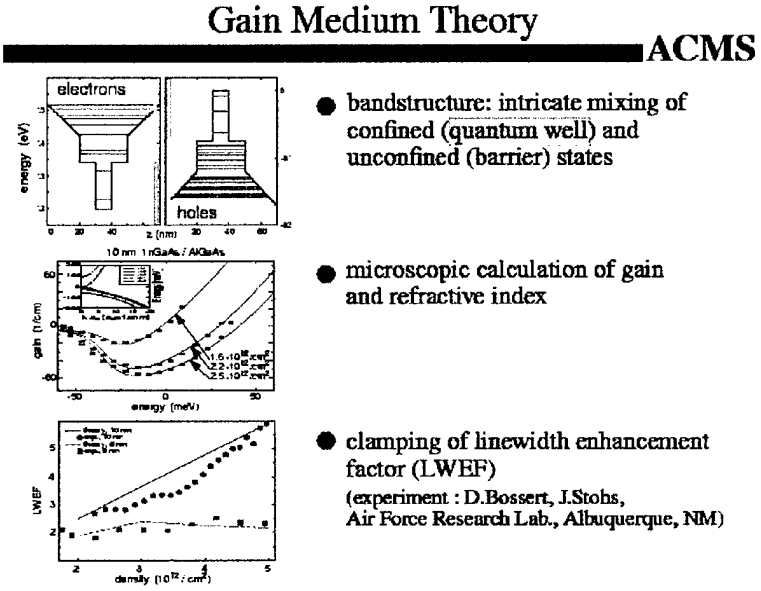

As an illustration, we ran a simulation of a broad area device for both QW structures at high pump levels and compared the time-averaged far-field outputs for the otherwise identical lasers. As the far-field outputs are steering randomly on sub-nanosecond time scales in these devices due to strong dynamic filamentation instabilities, only time-averaged quantities are meaningful. The figure on the right shows that the narrow QW structure (solid line) has an average far-field broadening which is about one half of the wider well device. This result confirms that our unique approach of building simulation tools on a predictive microscopic physics basis offers the possibility of designing and optimising device performance starting from the materials processing level.

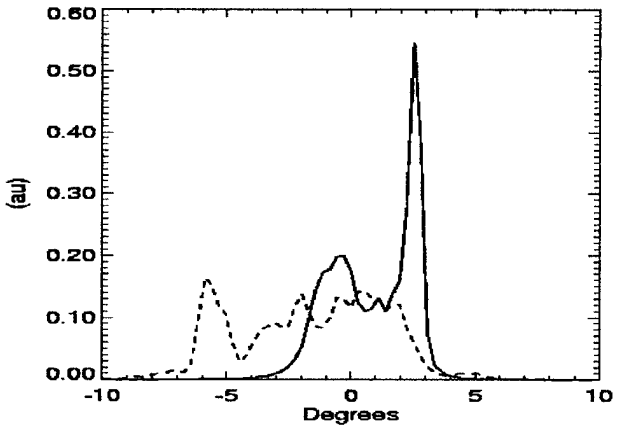

An Interactive Simulator for High Brightness Diode Lasers

Bouyed by successes such as the above, we have embarked on an ambitious program to build a fully interactive supercomputing simulator using parallel processing on our Silicon Graphics ONYX2 multi-processor graphical supercomputer. We are designing the interactive simulator in such a way that the user will be able to probe the system and change parameters on the fly. Pull-down menus will facilitate the utilization of tools to profile the pump current, refractive index profile and modify linear/curved gratings for wavefront control and surface emission.

A layout of the simulator is displayed in the picture to the right. Each layer in the structure indicates a particular design feature or instantaneous snapshots of the relevant physical fields being resolved within the active layer of the device. For example, it is straightforward to add contacts of general shape, grating sections etc. The picture shows two contacts defining the separate gain regions of

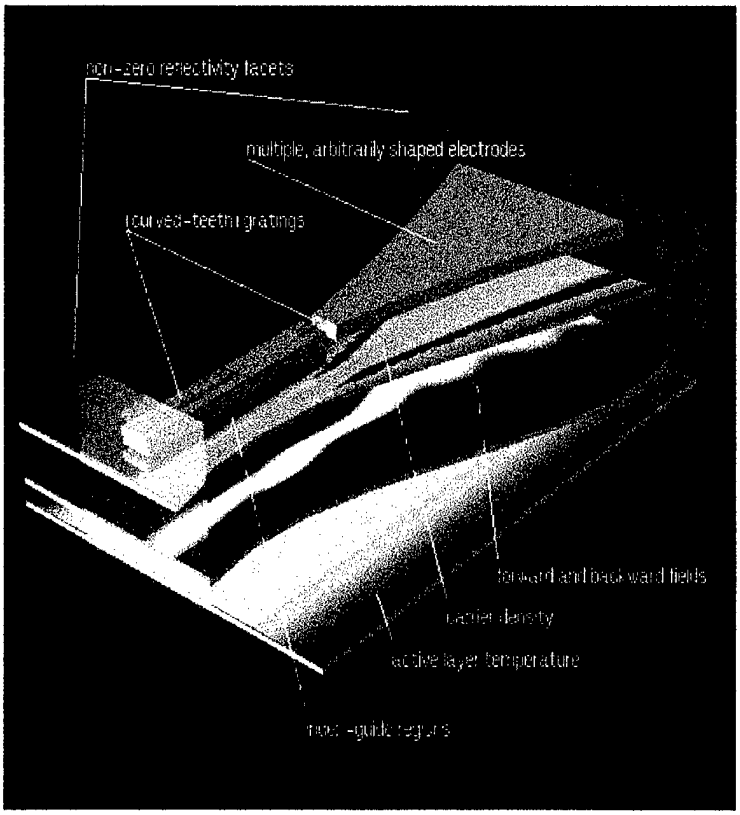

the device. The narrow straight contact has gratings at both ends to define a single lateral and longitudinal mode DBR master oscillator. The expanding flare from one end of the master oscillator is the power amplifier section. The facet reflectivities at the wide end of the flare can be varied and one usually assumes an AR coating with reflectivities as low as 0.0005. Even with such low reflectivity, the device can readily switch-on as a multi-mode laser when the master oscillator current is modulated. The layer beneath the contacts shows a contour of the instantaneous carrier density distribution thoughout the active layer region. The dark troughs at the edges of the expanding flare represent large unsaturated carrier densities and these are a major source of degradation of the far-field of this device. By adding current profiling and cavity spoilers, such devices can be pushed to higher output powers while retaining high brightness. This simulation tool is becoming an invaluable resource for future high brightness system design and optimization. A specific illustration of a high brightness laser design which utilizes current profiling and a cavity spoiler is shown in the picture on the right. The top left frame shows a the carrier density profile in a 3-contact bow-tie laser with a flat current pump profile throughout. The narrow central section is meant to act as a spatial mode filter and has a grating section for longitudinal mode filtering. A current of 100 mA is applied to this narrow contact and each flare has a current of 1.5 A. The lower picture on the left shows the identical device but now with a modified current profile and a cavity spoiler placed at the center of the narrow section. The shapes of the current profiles are shown to the right of each picture. The dark stripes at the edge of the flares in the top picture indicate the formation of regions of high unsaturated carrier density. These promote filamentation instabilities in the device and lead to significant far-field degradation. In addition the fuzzy areas outside the straight contact edges are regions where the optical intensity has bleached out the carriers and the gain material is transparent in these regions. Increasing the pump current leads to stronger bleaching and an increased tendency for filamentation. The profiled contact suppresses the growth of unsaturated carriers at the contact edges and the cavity spoiler acts as a lossy element for the bleached regions of the device. Consequently, the brightness of the lower device is considerably enhanced. This build-up of unsaturated carriers has been seen experimentally by the group of J. McInerney (Cork) in flared contact devices by imaging the spontaneous emission through a transparent contact on the surface of the device. This group has used an older version of our device simulation software to design profiled contacts and have demonstrated improved far-field emission in broad area devices [P.O'Brien, P.M.W. Skovgaard, J.G. McInerney and J.S. Roberts, Electron. Letts., **34**, 1943 (1998); P.M. W. Skovgaard, P. O'Brien and J.G. McInerney, Electron. Letts., **34**, 1950 (1998)]

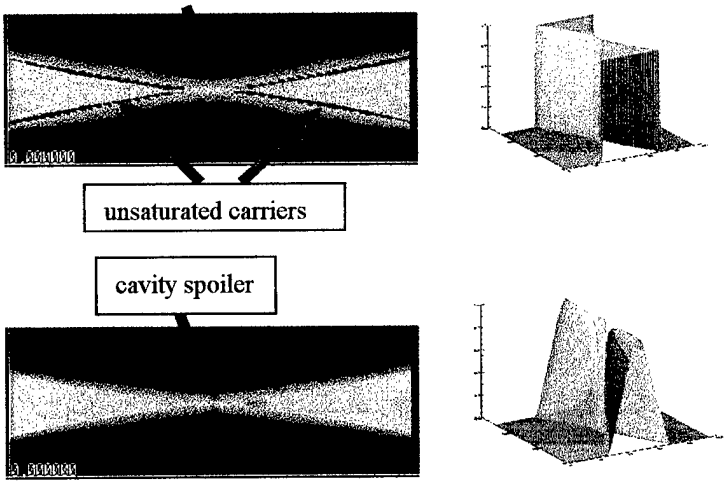

An Optoelectronic Systems Simulator

The gain spectra, once calculated for a specific structure, can be used as the active layer in a host of different geometry laser structures including high power edge/surface emitters, low power VCSEL:s and low power edge emitters typically employed in telecommunications systems. In telecommunications systems, the semiconductor lasers have strong lateral and transverse optical confinement and can be modelled as 1+1 D systems. This allows us to quantitatively resolve the multi-longitudinal mode behavior of a general device in a computationally fast and efficient manner. The semiconductor laser solver can now become an individual module in a sophisticated optical systems simulator and various other optical components in realistic telecommunications systems (DFB/DBR lasers, fibers, AR and HR coatings, beam splitters, external cavities, etc) can be built and accessed via pull-down menus within an optical systems graphical GUI editor. We embarked building this simulator at the beginning of the Fall semester 1999 and are making rapid progress in assembling the simulator. As the simulator is again built on a fully microscopic basis, it should become a powerful interactive simulation tool for designing conventional, soliton-based or novel chaos-based telecommunications systems. Our plan is to build a platform independent simulation tool which will take advantage of the rapid increase in CPU clock speeds of new generations of intermediate end graphical workstations. Ideally the simulator will require at least a dual CPU box with a high bandwidth communications interface so that the heavy parallel graphical diagnostics (intensity traces without and with detector averaging, power spectra, eye-diagrams etc) can be off-loaded from the computationally heavy core simulator. A rather primitive but working version of a simulator window is shown below.

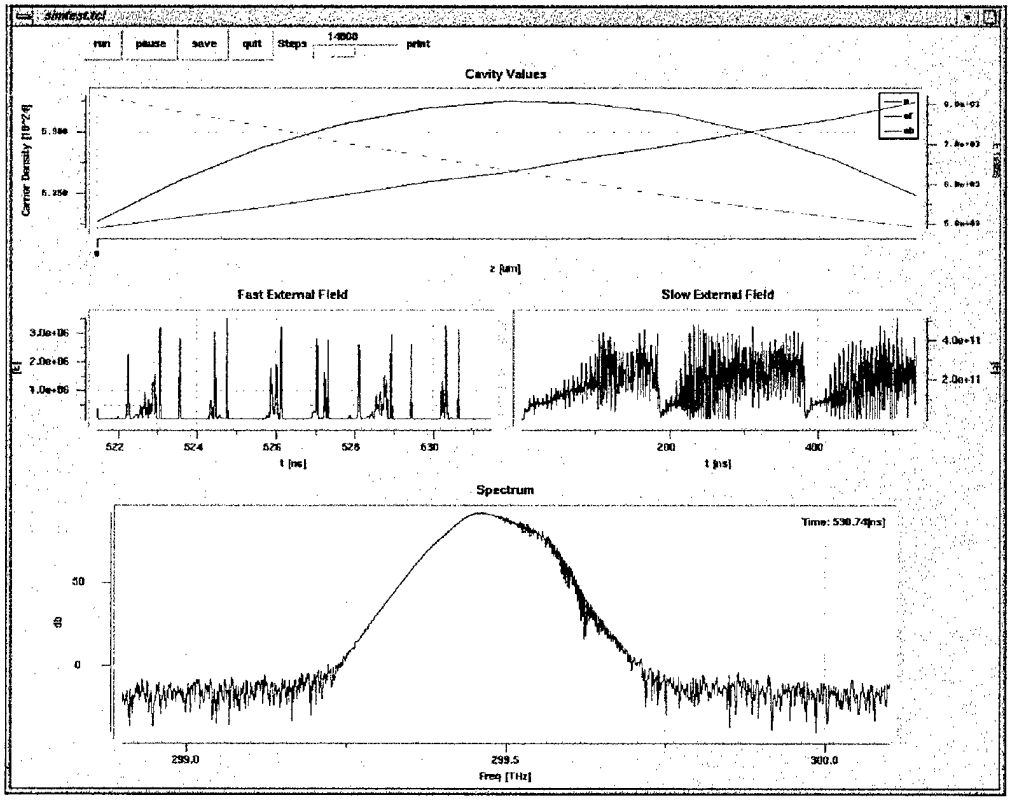

The top frame shows the z-resolved (laser axis) forward (red), backward (green) internal field intensities and the carrier density (blue) along the device. The left middle frame shows the finely resolved evolution of the laser output and the right middle frame a detector averaged response over a much longer time window. The bottom frame depicts the time evolution of the spectrum of the output field. The case depicted here is a short (single mode) laser cavity with an external reflector with a reflectivity of 1% placed about 1 m away from the original cavity. The feedback induces an instability in the device which manifests itself as a chaotic pulsing of the output (left middle frame) with pulse durations of about 15-20 ps. The coarse, detector averaged output shows the characteristic power dropouts of the device and the spectrum the extremely broad chaotic output spectrum.

High Power Femtosecond Light Strings

Our contract has enabled us to leverage a preliminary study of a very promising new field which has the potential of providing a broad base of important military and civilian applications opportunities. The ACMS group were the first to identify the highly dynamic mechanism by which a high power femtosecond-duration laser pulse can form a nonlinear waveguide in air [98-2]. The critical power for self-focusing in air is approximately 2 GW and an ultrashort laser pulse with incident powers exceeding this level can critically focus in air, causing optical breakdown at where the intensity becomes extremely high ($\approx 10^{13} - 10^{14}$ W/cm^2). A narrow plasma filament is created by the intense pulse with diameter ranging between 80μm (IR) to 120μm (UV) and of the order of a meter or longer in length. We identified the underlying physical mechanism for the formation of this light guide as a form of "dynamic spatial replenishment" whereby the pulse can undergo critical collapse (self-focusing) more than once within a single pulse. This dynamic mechanism is illustrated in the four frames in the picture on the right. The computation here was carried out in radial symmetry and the radial coordinate corresponds to the transverse coordinate in each frame. The coordinate along the pulse is the time coordinate. The pulse (top picture) first begins to self-focus on the leading edge and the collapse singularity is regularized by the generation of a narrow plasma filament which is left in the wake of the pulse i.e the plasma recombines on a ps time scale. The narrow plasma filament

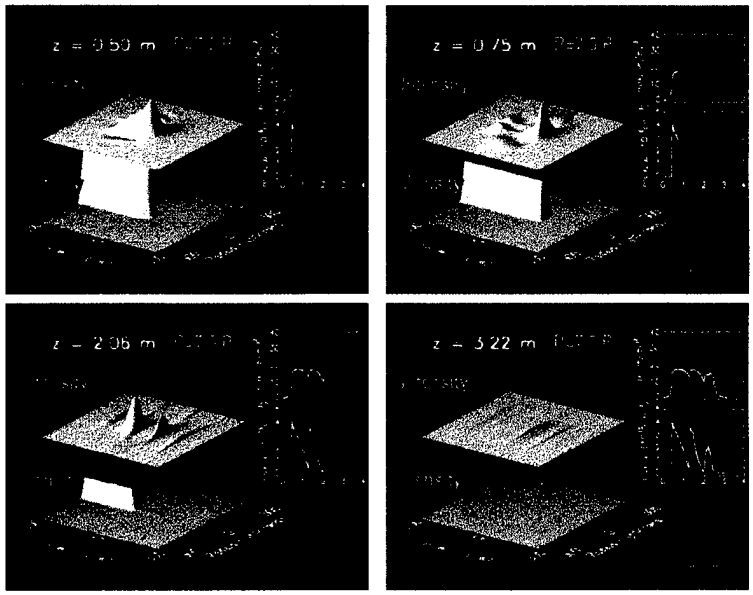

acts as a strongly defocusing lens which counteracts the self-focusing and strongly evacuates the light immediately behind the initial focus. The plasma turns off as the intensity drops and a secondary collapse can occur if the power behind the leading focus exceeds critical. This process can recur a number of times. Each occurrence leaves a narrow plasma filament in the wake of the intensity focus and these filaments recombine on a much slower scale.

When the power is cranked up such that the incident laser pulse contains tens to hundreds of critical powers the situation becomes extremely interesting. For example, an experiment by a group in Jena, Germany using a 2.5 TW 100 fs laser pulse were able to probe the upper atmosphere ($\approx$12 km) by delivering a white light continuum spectral probe from which they were able to detect absorption lines from various molecular species. In this experiment, the incident pulse contains on the order of 1000 critical powers. The key physics associated with this process is that femtosecond-duration pulses cause optical breakdown primarily via an instantaneous multi-photon rather than a cumulative avalanche process. Funding in the present contract helped us develop a sophisticated adaptive mesh, parallel algorithm which enabled us to drop the radial symmetry assumption above and extend our study to 3D + time [99-15]. Although we could not hope to simulate the Jena experiment, we were able to take pulses with tens of critical powers and demonstrate a fundamentally new physical phenomenon – the creation of optically turbulent light strings. The accompanying picture shows three separate time slices of the optical pulse and displays the chaotic creation of intensity "hot-spots" both across (via a modulational instability) and along (generalization of the radially symmetric "dynamic spatial replenishment" scenario) the pulse. Accompanying each light intensity focus is a plasma channel.

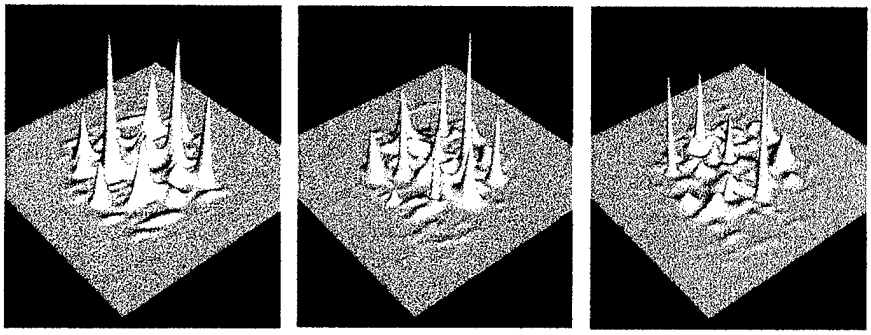

Air Force Links

Important collaborative links to the Air Force Research Laboratory in Albuquerque enabled us to fully test the microscopic many-body theory against structures that were completely characterized at the growth level. It is important to stress that this link with D. Bossert was crucial to our success in anchoring the combined bandstructure/many-body calculations as the growth details of most materials are not available to us and considered proprietary by industry. The experimentally measured gain, index and linewidth enhancement factor spectra on these QW devices enabled us to identify the mechanism behind the LWEF clamping.

Our group has also established direct links to the DELO branch (C. Denman and A. Gavrielides) on two projects. We have had preliminary meetings on modeling double clad optical fibers for

high brightness applications and this area has now been identified as a priority under our new contract award. Studies on chaotic dynamics of semiconductor lasers with external cavities were also undertaken by us [99-2] and we identified the important role of isolated laser longitudinal modes in offering a WDM chaotic synchronization and communications paradigm for a telecommunications system. We are currently in communication with A. Gavrielides at DELO and plan to use our optoelectronic simulator discussed above to implement a full chaotic communications interactive testbed.

Industrial Collaborations and Links

The present contract leveraged initial contacts with Opto Power Corporation in Tucson and led to the award of an NSF GOALI grant to work directly with this company. We are currently pursuing the development of flared high brightness surface emitting devices with Opto Power and the experimental group of Prof. M. Fallahi in Optical Sciences. A reprint of a recently submitted joint publication is attached.
An invited talk at the recent Advanced High Power Laser Applications international conference in Osaka, Japan by the PI has stimulated an enthusiastic response from semiconductor laser companies worldwide. Prior to this conference, we had established a direct contact to Dr. Kan, Director of Research at Hammatsu, Japan. Panasonic (USA), Osram (Germany) and the Fraunhofer Institute (Aachen, Germany) and its subsidiary, Fraunhofer USA, Center for Laser Technology, Plymouth, MI 48170, USA, were particularly interested in our novel approach of combining the microscopic physics and full scale interactive simulation. We are currently pursuing a collaborative link to with the latter three groups.

Key Personnel Supported

U. of A. Faculty:

J.V. Moloney (Math, PI)
N. Ercolani (Math, Co-PI)
R.A. Indik (Math, Co-PI)
R. Binder (Optical Sciences)
E.M. Wright (Optical Sciences)
J. Lega (Math)
J. Xin (Math)

External Faculty:

S.W. Koch (Marburg, Germany and Adjunct Professor, Optical Sciences)
J.G. McInerney (University College Cork and Adjunct Professor, Optical Sciences)
N. Bloembergen (Harvard and Nobel Laureate)

Postdoctoral Fellows:

J. Hader
M. Kolesik
M. Mlejnek (now with Corning)
K. Kasunic
T. Roessler (now with Siemens)
J.-F. Mercier (now with CNRS, France)
D. Burak (now with Agilent Technologies)

Graduate Students:

M. Matus
K. Gross (AASERT)
H.J. Han
D. Hochheiser (AASERT)
J.K. White (AASERT, now with Nortel Networks)
R. Gatifovich
J. Auxier

Other Investigators, Collaborators and Contacts

Semiconductor Laser Branch (PL/LIDD)
Maj. Greg Vansuch
M. Wright
D. Bossert
Nonlinear Optics Group (PL/LIDD)
A. Gavrielides
A. Kovanis
A. Hohl
Lincoln Labs
J. Walpole

Opto Power Corporation
S. Yang
S. Macomber
S. Srinivasan
Philips Research (Eindhoven)
L. Spiekman
G. Van Tartwyk
University College Cork
J. McInerney
Wright Patterson Laboratory
Dr. Ed Watson
Dr. Paul F. McManamon

Publications

97-14 Y.V. Lvov and A.C. Newell, "Semiconductor Lasers and Kolmogorov Spectra," *Phys. Letters A* **235**, pp. 499-503 (1997).

97-15 C.Z.Ning, R.A. Indik, and J.V. Moloney, "Effective Bloch Equations for Semiconductor Lasers and Amplifiers," *IEEE-JQE,* **33** (9), pp. 1543-1550 (1997).

97-16 P.M.W. Skovgaard, J.G. McInerney, J.V. Moloney, R.A. Indik, and C.Z. Ning, "Enhanced Stability of MFA-MOPA Semiconductor Lasers Using a Nonlinear, Trumpet-Shaped Flare," *IEEE Photonics Technology Letters* **9**(9), pp. 1220-1222 (1997)

98-1 A. Egan, C.Z. Ning, J.V. Moloney, R.A. Indik, M.W. Wright, D.J. Bossert, and J.G. McInerney, "Dynamic Instabilities in MFA-MOPA Semiconductor Lasers," *IEEE JQE,* **34**(1), pp. 166-170 (1998).

98-2 M. Mlejnek, E.M. Wright, and J.V. Moloney, "Dynamic Spatial Replenishment of Femtosecond Pulses Propagating in Air," *Optics Letters* **23**(5), pp. 382-384 (1998).

98-3 C.Z. Ning, S. Bischoff, S.W. Koch, G.K. Harkness, J.V. Moloney, and W.W. Chow, "Microscopic Modeling of Vertical-Cavity Surface-Emitting Lasers: Many-Body Interaction, Plasma Heating, and Transverse Dynamics," *Optical Engineering* **37**(4), pp. 1175-1181 (1998).

98-4 J.K. White, J.V. Moloney, A. Gavrielides, V. Kovanis, A. Hohl, and R. Kalmus, "Multi-Longitudinal Mode Dynamics in a Semiconductor Laser Subject to Optical Injection,'" *IEEE JQE* **34**(8), pp.1469-1473 (1998).

98-5 J.V. Moloney, A.Egan, C.Z. Ning, and R.A. Indik, "Spontaneous Spatiotemporal Instabilities in Current Modulated Master Oscillator Power Amplifier Lasers," *IEEE Photonics Technology Letters* **10**(9), pp. 1229-1231 (1998).

98-6 T. Rössler, J.K. White, R. A. Indik, and J.V. Moloney, "Multimode Nonlinear Dynamics in Semiconductor Lasers: From Patterns to Chaos," *Asian Journal of Physics* **7**(3), pp. (insert later) (1998).

98-7 A.J. Kent, A. Egan, J.G. McInerney, and J.V. Moloney, "Enhanced Diffraction Limited Output Power of Tapered Gain Semiconductor Lasers," *Optics Press* Web Publication (Online *Optics Journal*) 2(12), pp. 509-514 (1998).

98-8 JV Moloney, "Ultrafast Intense Probes of Nonlinear Optical Material Interactions," *Nonlinear Optical Materials* Workshop Proceedings, The IMA Volumes in Mathematics and its Applications, Springer-Verlag (101), pp. 177-204 (1998).

98-9 J. Xin and J. V. Moloney, "Global Solutions and Attractors of a Maxwell-Bloch Raman Laser System in Two Transverse Dimensions," *Nonlinearity* 11, pp. 501-5271 (1988).

98-10 M. Mlejnek, E.M. Wright, and J.V. Moloney, "Femtosecond Pulse Propagation in Argon - A Pressure Dependence Study," *Physical Review E* **58**(3) (1998).

98-11 T. Rössler, R.A. Indik, G.K. Harkness, and J.V. Moloney, "Modeling the Interplay of Thermal Effects and Transverse Mode Behavior in Native-Oxide Confined Vertical-Cavity Surface-Emitting Lasers," *Physical Review A* **58** (4), pp. 3279-3292 (1998).

98-12 R.F. Pawula, "A New Formula for MDPSK Symbol Error Probability," *IEEE Communications Letters* **2**(10), pp. 271-272 (1998).

98-13 Y. Lvov, R. Binder, and A.C. newell, "Quantum Weak Turbulence in Application for Semi-conductor Lasers, *Physica D* **121**, pp. 317-343 (1998).

98-14 M. Mlejnek, E.M. Wright,and J.V. Moloney, "Long Distance Propagation in Air Due to Dynamic Spatial Replenishment," *Optics and Photonics News* **9**(12) pp.38-39 (1998).

99-1 J.V. Moloney, "Spontaneous Generation of Patterns and Their Control in nonlinear Optical Systems," *J. Opt. B: Quantum Semiclass* **1**, pp. 183-190 (1999).

99-2 J.K. White and J.V. Moloney, "Multichannel Communication using an Infinite Dimensional Spatiotemporal Chaotic System," *Phys. Review A* **59**(3), pp. 2422-24226 (1999).

99-3 N. Bloembergen, M. Mlejnek, J.V. Moloney, and E.M. Wright, "Femtosecond Pulses at the

Boundary of a Nonlinear Dielectric," *Advances in Laser Physics* ed. By V.S. Lethokov and P. Meystre, a Festschrift in the honor of Peter Franken on his 70th Birthday, Gordon & Breach (in press) (1999).

99-4 J.V. Moloney, "Coherent Structures in Dissipative nonlinear Optical systems," *Nonlinear Science at the Dawn of the 21st Century*, ed. P.L. Christiansen and M.P. Soerenson, and A.C. Scott, *Springer-Verlag*, pp. 229-246 (1999).

99-5 J. Hader, D. Bossert, J. Stohs, W.W. Chow, S.W. Koch, and J.V. Moloney, "Clamping of the Linewidth Enhancement Factor in Narrow Quantum-Well Semiconductor Lasers," *Appl. Phys. Lett.* **74**(16), pp. 2277-2279 (1999).

99-6 M. Mlejnek, E.M. Wright, and J.V. Moloney, "Power Dependence of Dynamic Spatial Replenishment of Femtosecond Pulses Propagating in Air," *Optics Press Web Publication* (Online Optics Journal) **4**(7), pp. 223-228 (1999).

99-7 R.F. Pawula, "Generic Error Probabilities," *IEEE Transactions on Communications* **47** (5), pp. 697-702

99-8 M.Mlejnek, E.M. Wright, and J.V Moloney, "Moving-Focus Versus Self-Waveguiding Model for Long Distance Propagation of Femtosecond Pulses in Air," *IEEE Journal of Quantum Electronics,* **35**(12) pp. 1771-1776 (1999).

99-9 L. Gilles, J.V. Moloney, and L. Vazquez, "Electromagnetic Shocks on the Optical Cycle of Ultrashort Pulses in Triple-Resonance Lorentz Dielectric Media with Sub-Femtosecond Non-linear Electronic Debye Relaxation," *Phys. Review E* **60**(1), pp. 1051-1059 (1999).

99-10 J.V. Moloney, R.A. Indik, J. Hader, and S.W. Koch, "Modeling Semiconductor Amplifiers and Lasers: From Microscopic Physics to Device Simulation." *JOSA B*, **16**(11) pp. 2023-2029 (1999).

99-11 M. Mlejnek, M. Kolesik, J.V. Moloney, and E.M. Wright, "Optically Turbulent Femtosecond Light Guide in Air." *Phys. Review Letters*, **83**(15) pp. 2938-2941 (1999).

99-12 J.V. Moloney, M. Kolesik, J. Hader, and S.W. Koch, "Modeling High-Power Semiconductor Lasers from Microscopic Physics to Device Application" *SPIE Proceedings* (in press) (1999).

99-13 J. Hader, J.V. Moloney, and S.W. Koch, "Microscopic Theory of Gain, Absorption and Refractive Index in Semiconductor Laser Materials--Influence of Conduction-Band Nonparabolicity and Coulomb-Induced Intersubband Coupling." *IEEE-JQE.* **35** (12) pp 1878-1886 (1999)

99-14 R.F. Pawula, "Improved Performance of Coded digital FM," *IEEE Trans. on Comm.* **47**(11),

pp. 1701-1708, (1999).

99-15 M. Mlejnek, J.V. Moloney, E.M. Wright, and N. Bloembergen, "Second Harmonic Boundary of a Nonlinear Dielectric (Peter Franken's original experiments revisited), *Physical Review Letters* **83**(15), pp. 2934-2937 (1999).

Tapered-Cavity Surface-Emitting Distributed-Bragg-Reflector Semiconductor Lasers: Modeling and Experiment

H. Luo, K. J. Kasunic*, S. H. Macomber†, R. Bedford, J. V. Moloney*, and M. Fallahi

Optical Sciences Center, University of Arizona,

1630 E. University Blvd., Tucson, AZ 85721

luoh@u.arizona.edu

Keywords

Laser modeling, semiconductor lasers, surface-emitting lasers, tapered lasers, DBR lasers

Abstract

We report on the design and fabrication of tapered cavity grating coupled surface-emitting DBR lasers in the 980-nm regime. A curved second order grating is used at the end of a tapered gain section to provide feedback as well as collimated surface out-coupling. A detailed numerical analysis shows a far-field central lobe power of 75% is possible up to twice threshold. Near diffraction-limited collimated surface-emitting output with moderate power of about 150 mW is obtained under continuous operation.

* Department of Mathematics, University of Arizona, Tucson, AZ 85721.
† Opto Power Corporation, 3371 East Global Loop, Tucson, AZ 85706

I. INTRODUCTION

High brightness semiconductor lasers are important light sources for applications such as pumping of EDFAs, Raman amplifiers, and for free space optical communications. In order to obtain high power from a semiconductor laser, a large aperture is needed to avoid the problems of optical damage and high current density operation. However, wide aperture lasers undergo rapid filamentation and multi-lateral mode operation. To prevent multi-lateral mode oscillation, some method of mode discrimination is needed. To date, the most reliable concepts have been the master oscillator power amplifiers (MOPAs) and unstable resonator lasers. High power single mode operation has been reported in both of these edge-emitting devices [1]-[3]. However, due to their high degree of anamorphicity and astigmatism in the output beam, coupling of these lasers to a single-mode waveguide or fiber is problematic. Highly specialized, high numerical aperture optics are required for efficient coupling into single-mode fibers.

To alleviate the need for external optics and related optomechanical alignment problem, grating-coupled surface-emitting lasers (GCSEL) can be used. In comparison to edge-emitting lasers, surface-emitting devices have several advantages: low divergence angle, compatibility with beam forming elements, single-longitudinal mode operation, on wafer testing and 2-D array integration. Based on the feedback grating configurations, GCSELs can be divided into two types: the first uses first-order grating for feedback and detuned second-order grating for out-coupling, the second uses a single second-order Bragg grating for both feedback and out-coupling. The first configuration separates the out-coupler from the oscillator and gives the maximum flexibility [4]. However, because

feedback and out-coupling have different grating periods, they may experience wavelength detuning and beam steering as operating condition changes. The second configuration combines the feedback and out-coupling into a single second-order Bragg grating. While the beam-forming capability is somehow limited in this configuration, stable normal to the surface out-coupling is intrinsically guaranteed without any beam steering [5]. In addition, by matching the curvature of the second order grating to the phase front of the forward propagating wave, collimated outcoupling beam can be achieved. Finally due to the fact that the emitting aperture is significantly larger than the edge-emitting laser, catastrophic optical damage can also be greatly reduced.

Here we study the design of a tapered cavity surface-emitting laser with a curved grating. The paper is organized as follows: in section II we present the numerical analysis based on a comprehensive semiconductor laser modeling. Section III describes the design and fabrication of the laser. In section IV the experimental results are described. We then present discussion and concluding remarks in section V.

II. MODELING

The schematic illustration of the tapered cavity surface-emitting DBR laser is shown in Fig. 1. The laser consists of an index-guided ridge waveguide followed by a gain-guided tapered section. A curved second-order Bragg grating provides feedback and surface-emission while the other facet can be defined by cleaving. The results obtained with the tapered DBR resonator shown in Fig. 1 will depend strongly on the curvature and in-plane reflectivity of the second-order grating used on the flared end of the resonator. To

obtain a narrow far-field pattern, for example, this grating must be designed to match the wavefront curvature of the beam from the ridge waveguide on the far end of the flare, thereby requiring a semi-stable resonator configuration. Unfortunately, the strength of the resulting counter-propagating field increases the tendencies toward filamentation typically found in broad-area semiconductor devices [6]-[9].

These tendencies can be strongly attenuated with an unstable-resonator design. First proposed for Fabry-Perot cavity [10] [11], these devices achieved brightness levels on the order of 20-30 times greater than that for stable cavities. Typical magnifications for such performance are approximately 2 to 3 [12], with greater magnifications leading to larger losses and therefore lower efficiencies. O'Brien extended these concepts to the case of an edge-emitting flared unstable resonator using straight-line distributed-Bragg-reflectors (DBRs) to define the cavity [13]. As shown below, the mismatch between the grating and field curvatures results in extremely large far-field angles if this unstable resonator is used in a surface-emitting geometry. Thus our design is a compromise between a filament-resistant unstable cavity and the potential for a diffraction-limited beam for lower-power operation with the semi-confocal curved-grating cavity.

In this section, we present numerical results showing the sensitivity of far-field beam size to power level. Our approach is to first find a grating curvature that produces a narrow far field at a specific pumping current; we then increase the power level with the expectation that carrier-induced refractive index changes will modify the power in the side lobes. Our model has been described in detail previously, and includes the effects of counter-propagating fields, lateral diffraction, carrier diffusion, and a comprehensive gain

model that incorporates many-body effects [14] [15]. Gain/index coupling via the linewidth enhancement factor α is inherent in the gain model; no explicit input of a spatially averaged factor is required. Including curved-grating effects and neglecting gain and absorption features described previously [15], the forward and backward-propagating field envelopes $F(x,z,t)$ and $B(x,z,t)$ in the grating region are given by

$$\frac{1}{v_g}\frac{\partial F(x,z,t)}{\partial t}+\frac{\partial F(x,z,t)}{\partial z}=\frac{i}{2k}\frac{\partial^2 F(x,z,t)}{\partial x^2}-\varepsilon F(x,z,t)+(i\kappa-\varepsilon)B(x,z,t)e^{ikx^2/R(z)} \quad (1)$$

$$\frac{1}{v_g}\frac{\partial B(x,z,t)}{\partial t}-\frac{\partial B(x,z,t)}{\partial z}=\frac{i}{2k}\frac{\partial^2 B(x,z,t)}{\partial x^2}-\varepsilon B(x,z,t)+(i\kappa-\varepsilon)F(x,z,t)e^{-ikx^2/R(z)} \quad (2)$$

where x and z are the lateral and longitudinal coordinates, v_g is the group velocity, $k=\omega n_{eff}/c$ is the magnitude of the field wavenumber, κ is the in-plane coupling coefficient, ε is the outcoupling coefficient for surface emission, and $R(z)$ is the z-dependent radius of curvature for a concentric circular grating. Note that the quadratic phase factor applies only in the paraxial regime typical of the ten degrees flare angle found in most tapered devices. Also note that the carrier density and electronic polarization equations are not affected by the curved grating.

To obtain far-field intensity profiles, we first propagate Eqs. (1) and (2) for about 10 nanoseconds, allowing time for oscillations to settle. We then obtain a near-field amplitude profile $E_N(x,z)$ consisting of

$$E_N(x,z)=F(x,z)e^{-ikx^2/2R(z)}+B(x,z)e^{ikx^2/2R(z)}$$

where the phase of $F(x,z)$ and $B(x,z)$ are corrected for the way in which the grating out-diffracts the in-plane wavefront. The far-field intensity is then obtained from the magnitude-squared of the Fourier transform of $E_N(x,z)$.

The far-field intensity outcoupled from a linear grating at the end of the flare is shown in Fig. 2. For this geometry, $R(z)=\infty$ for all z, so no correction occurs in Eqs. (1) and (2). The resulting phase mismatch between the field and grating curvature results in an enormous far field in comparison with the 0.38 degree full-width at half-maximum (FWHM) diffraction limit for a 150 μm aperture. The simulation assumes $\kappa = \varepsilon = 10cm^{-1}$ for the coupling coefficients; the gain medium is a 10 nm InGaAs quantum well (QW) sandwiched between graded index $Al_xGa_{1-x}As$ layers, where x varies from 0.1 to 0.6 over a distance of 85 nm.

For a circular curved grating, on the other hand, with an inner radius that approximately matches the length of the flare, Fig. 3 shows that a near-diffraction-limited spot size with reasonable side lobes is obtained close to threshold (1.03 J_{th}). At higher power, we expect the α-factor to change the wavefront curvature from its near-threshold value, thus affecting the far-field profile. Simulations show that, excluding thermal effects, this does not become important until about twice threshold. Above this, the temporal oscillations do not settle. Dynamic instabilities, possibly of the type described by Lowery [16], are observed numerically. As shown in Fig. 4, the on-axis beam angle at a particular time can retain it's low-divergence character; unfortunately, the increase in side-lobe intensity decreases the fraction of power in the central lobe (or power in the bucket) to 67% (from 80% in Fig. 3). The asymmetry in the far field is indicative of the

temporal variations at this power level (2.05 J_{th}). Note that at even higher powers, the resulting far-field intensity is significantly degraded (Fig. 5) and again varying with time.

To summarize: a curved grating at the end of the flare is essential for a diffraction-limited spot. Assuming a reduction in central lobe power to about 75% and a small DFB outcoupling coefficient is acceptable for a given application, a reasonable power variation is then possible. Given the huge design "space", including pumping current, radius of the curved grating, grating shape (which we have not considered here), outcoupling and in-plane DFB coupling coefficients, and linewidth enhancement factor, our simulations show the possibility of obtaining a narrow-angle, surface-emitting beam up to about twice threshold.

III. DESIGN AND FABRICATION

The 3-μm wide ridge is designed to only support the fundamental lateral mode. The ridge length is 400-μm. Close to the junction between the ridge and the tapered section are two spoiling grooves located at the two sides of the ridge. The function of the spoiling groove is to prevent any feedback from the tapered section to the unpumped region in the ridge side. Therefore the ridge and spoiling groove combination functions like a spatial mode filter, which will promote the fundamental mode and suppress high order lateral modes. Follow the ridge is the tapered section, which provides most of the gain needed for lasing. The length of the tapered section is 1800-μm, and the end width of the taper is 225-μm. The taper has a full angle of about 7 degree, which is designed to accommodate the free diffraction of the beam inside the tapered section. The resonator consists of a

cleaved mirror on the ridge side and a curved second-order Bragg grating on the tapered side. The cleaved mirror is HR-coated to decrease the lasing threshold and to increase the out-coupling efficiency on the grating side. The second-order grating provides both feedback and surface out-coupling. The curvature of the grating is designed to approximately match the phase front of the forward propagating beam, in this case, the center of curvature is located at 1800 μm from the tapered end. This will collimate the output beam so that it has a small divergence angle.

The devices were fabricated from a strained InGaAs/GaAs three-quantum well GRINSCH structure. The layer structure consists of a 1.5-μm thick n-$Al_xGa_{1-x}As$ (x~60%) cladding layer, a 0.12-μm thick undoped $Al_xGa_{1-x}As$ (x~60%-25%) GRIN optical confinement layer, three 6-nm InGaAs quantum wells with 20-nm GaAs barrier, a 0.12-μm thick $Al_xGa_{1-x}As$ (x~60%-25%) GRIN optical confinement layer, a 0.3-μm thick p-$Al_xGa_{1-x}As$ (x~60%) cladding layer, a 10-nm GaAs etch-stop layer, 0.9-μm thick p-$Al_xGa_{1-x}As$ (x~60%) cladding layer, and a 0.1-μm thick p^+-GaAs cap layer.

First, the top contact (Ti/Pt/Au) for the ridge and tapered section is formed by lift-off process. The ridge section and grating section are simultaneously etched down by electron-cyclotron-resonance-reactive-ion etching (ECR-RIE). The etch-depth is controlled by timing to ensure that the etching stops about 0.1-0.2 μm- above the etch-stop layer. A selective wet etching is then used to remove the remaining AlGaAs down to the GaAs etch-stop layer. Here the inclusion of an etch-stop layer is important. It allows us to perfectly control the fabrication of the ridge so the lateral mode profile can be ensured. It also enables us to control the position of the grating with great accuracy. After

the grating area is etched down to the etch-stop, curved second order Bragg gratings are defined by electron beam lithography. Since the grating section is identical to the gain section (no regrowth), the grating period is designed so the lasing wavelength is slightly red-shifted from the gain peak. This is necessary to reduce absorption losses in the passive section. This choice however makes the lasing less efficient. It also increases the α-factor, which may cause a tendency towards filamentation. The gratings are then etched by a second ECR-RIE. The etch-depth of the grating is about 150 nm. After that spoiling grooves are defined by wet etching. The etching is timed to etch through the active region to prevent any unwanted feedback. The device is then lapped in the backside down to about 100-μm total thickness. A Ni/Ge/Au n-side metallization is then deposited. The device is annealed using rapid thermal annealing (RTA) to form an ohmic contact. The device is cleaved on the ridge side and the mirror is coated for a reflectivity of about 90%. Finally, the device is bonded p-side up on a gold plated 14-pin mount and wire-bonded for testing.

IV. EXPERIMENTAL RESULTS

The device is tested at room temperature under pulsed and continuous operation. The laser is placed p-side up on a copper plate whose temperature is controlled. Since the laser is die-bonded p-side up, the thermal resistance is expected to be very high. For the pulsed operation, the pulse-width is fixed at 5-μs, and the duty-cycle is changed to investigate the thermal effect. The L-I characteristic under pulse operation with duty-cycle of 1% and 10% are shown in Fig. 2. There is little difference between these two

duty-cycles. Under the pulsed operation, the threshold current is 650 mA (corresponding to a threshold current density of 315A/cm^2) and the external differential quantum efficiency is 24.4%. Output power of 120 mW is obtained under the pulsed operation at a pump current of 1 A, which is the limit of our pulse current source. There is no sign of degradation, which indicates that higher power is possible at higher current. The laser is then tested under continuous operation with p-side up. The L-I curve under CW is also shown in Fig. 2. The threshold current is 700 mA (corresponding to a threshold current density of 339A/cm^2) and the external differential quantum efficiency is 15.5%. Output power of 150 mW is obtained under CW operation at a pump current of 1.5 A. The peak output power is limited by the thermal rollover as the current goes higher. The drop of the efficiency and power under CW compared to pulsed operation is also observed in other p-side up mounted broad-area lasers. This is mostly due to the large thermal effect under CW operation.

To investigate the beam-quality of the device, its far field at different driving currents is measured. The far field is measured by directly recording the beam on a CCD camera 200 mm away from the near field. This measurement setup does not correct any residual phase curvature that may be present in the near field, so this method measures the "true" divergence-angle of the far field. The measured far-field patterns under CW operation at different currents are shown in Fig. 3. Below 1.3 A (1.9 I_{th}), the far field had only one spot. As the current increases from the threshold up to 1.1 A (1.6 I_{th}) the divergence angle of the beam stays below 0.25°(FWHM), which corresponds to 1.1 times diffraction limited value for a 225 μm wide grating. As the current increases further, the

divergence angle increases slowly. The divergence angle increases to 0.30° at 1.3 A, which corresponding to approximately 1.4 times diffraction limited. As the current increases beyond 1.3 A, a second lobe starts to appear and the far field does not maintain a single lobe. We believe the increase of the divergence angle is mostly due to the thermal lensing effect. More efficient heat sinking and better packaging should increase the range of the current for near diffraction-limited operation.

V. CONCLUSION

We have carried out a detailed numerical analysis of a surface-emitting laser with curved gratings. The simulation results show that a near-diffraction limited collimated beam can be obtained within a reasonable range of applied current. We have fabricated and characterized such a laser. The device maintains near diffraction-limited operation up to 1.9 times threshold with far field divergence angle less than 0.3° (FWHM). A surface-emitting power of 150 mW is obtained under continuous wave operation.

Improvements can be made in several ways. Using bandgap-shifting technique, we can design the grating so the lasing wavelength is at the gain peak. This will increase the device efficiency. It will also decrease the α-factor and suppress filamentaion. Better heatsink and packaging can be used to decrease the thermal effect and improve the device performance at higher current.

ACKNOWLEDGEMENT

The authors appreciate discussions with Dr. R. A. Indik of University of Arizona's Department of Mathematics. This work was supported in part by the National Science Foundation's GOALI program under grant number DM59811466 and AFOSR under contract number F49620-97-1-0002 and F49620-98-1-0227.

References

[1] J. N. Walpole, "Semiconductor amplifiers and lasers with tapered gain regions," *Opt. Quantum Electron.*, vol. 28, pp. 623-645, 1996.

[2] S. O'Brien, D. F. Welch, R. A. Parke, D. Mehuys, K. Dzurko, R. J. Lang, R. Waarts, and D. Scifres, "Operating characteristics of a high-power monolithically integrated flared amplifier master oscillator power amplifier," *IEEE J. Quantum Electron.*, vol. 29, pp. 2052-2057, 1993.

[3] D. Mehuys, S. O'Brien, R. J. Lang, A. Hardy, and D. F. Welch, "5 W, diffraction-limited, tapered-stripe unstable resonator semiconductor laser" *Electron. Lett.*, vol. 30, pp. 1855-1856, 1994.

[4] N. Eriksson, P. Modh, and A. Larsson, "Grating-coupled surface-emitting laser with a hyperbolic unstable resonator producing a stable focus output beam," *IEEE Photon. Technol. Lett.*, vol. 11, pp1366-1368, 1999.

[5] S. H. Macomber, J. S. Mott, B. D. Schwartz, R. S. Setzko, J. J. Powers, P. A. Lee, D. P. Kwo, R. M. Dixon, and J. E. Logue, "Curved-grating, surface-emitting DFB lasers and arrays," in *Proc. Soc. Photo-Optical Instrumentation Engineers*, vol. 3001, pp. 42-54, 1997.

[6] A. Egan, C. Ning, J. Moloney, R. Indik, M. Wright, D. Bossert, and J. McInerney, "Dynamic instabilities in master oscillator power amplifier semiconductor lasers," *IEEE J. Quantum Electron.*, vol 34, pp. 166-170, 1998.

[7] M. Tamburrini, L. Goldberg, and D. Mehuys, "Periodic filaments in reflective broad area semiconductor optical amplifiers," *Appl. Phys. Lett.,* vol. 60, no.11, pp. 1292-1294, 1992.

[8] R. J. Lang, A. G. Larsson, and J. G. Cody, "Lateral modes of broad area semiconductor lasers: theory and experiment," *IEEE J. Quantum Electron.*, vol. 27, pp. 312-320, 1991.

[9] J. Salzman, T. Venkatesan, R. Lang, M. Mittelstein, and A. Yariv, "Unstable resonator cavity semiconductor laser", *Appl. Phys. Lett.*, vol. 46, pp. 218-220, 1985.

[10] M. Tilton, G. Dente, A. Paxton, J. Cser, R. DeFreez, C. Moeller, and D. Depatie, "High power, nearly diffraction-limited output from a semiconductor laser with an unstable resonator," *IEEE J. Quantum Electron.*, vol. 27, pp. 2098-2108, 1991.

[11] R. Defreez, Z. Bao, P. Carleson, M. Felisky, and C. Largent, "High-brightness unstable resonator semiconductor lasers", *Proc. SPIE*, vol. 1850, pp. 75-83, 1993.

[12] S. A. Biellak, C. G. Fanning, Y. Sun, S. S. Wang, and A. E. Siegman, "Reactive-ion-etched diffraction-limited unstable resonator semiconductor lasers," *IEEE J. Quantum Electron.*, vol. 33, pp. 219-230, 1997.

[13] S. O'Brien, D. Mehuys, R. J. Lang, and D. F. Welch, "1W CW single frequency, difraction-limited unstable resonator semiconductor laser with distributed Bragg reflector mirrors," *Electron. Lett.*, vol. 31, no. 3, pp. 203-205, 1995.

[14] C. Z. Ning, R. A. Indik, and J. V. Moloney, "Effective Bloch equations for semiconductor lasers and amplifiers," *IEEE J. Quantum Electron.*, vol. 33, pp. 1543-1550, 1997.

[15] J. V. Moloney, R. A. Indik, J. Hader, and S. W. Koch, "Modeling semiconductor amplifiers and lasers: from microscopic physics to device simulation," *J. Opt. Soc. Am. B.*, vol. 16, pp. 2023-2029, 1999.

[16] A. J. Lowery, "Dynamics of SHB-induced mode instabilities in uniform DFB semiconductor lasers," *Electron. Lett.*, vol. 29, no. 21, pp. 1852-1854, 1993.

Figure Captions

Figure 1: Schematic top view of a grating coupled tapered surface emitting laser.

Figure 2: Calculated far field intensity profiles scattered perpendicular to the surface of a linear grating.

Figure 3: Lateral far field intensity profile for a circular curved grating at 1.03 times the threshold current J_{th}.

Figure 4: Lateral far field intensity profile for a circular curved grating at 2.05 J_{th}.

Figure 5: Lateral far field intensity profile for a circular curved grating at 3.08 J_{th}.

Figure 6: Light-current characteristics of the surface-emitting laser.

Figure 7: Far field of the surface-emitting laser.

(a) I = 1.1 A (1.6 I_{th}), $\theta_{FWHM} = 0.25^{o}$ (1.1 D.L.).

(b) I = 1.3 A (1.9 I_{th}), $\theta_{FWHM} = 0.30^{o}$ (1.4 D.L.).

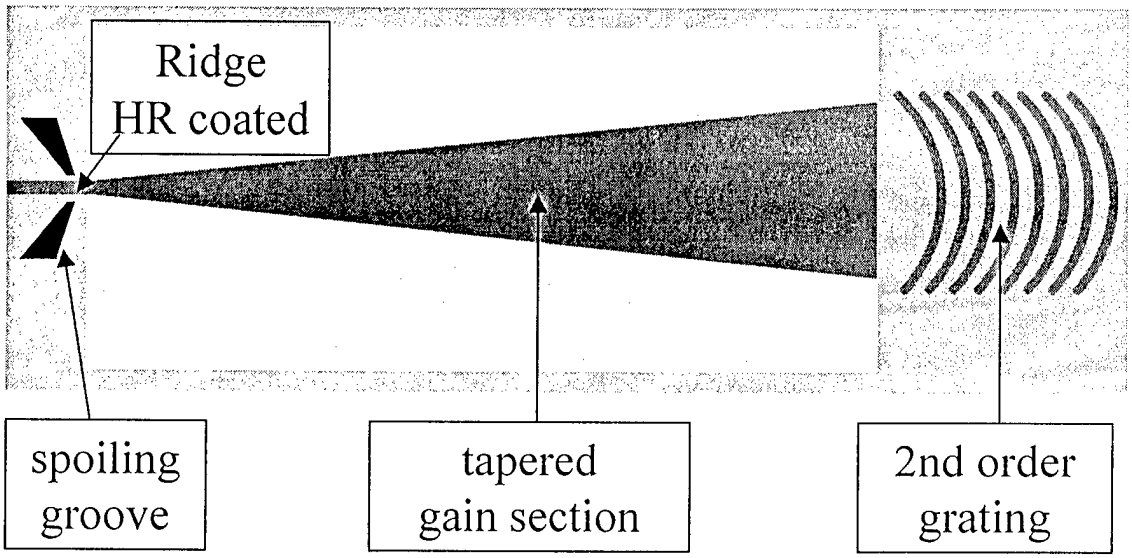

FIG. 1

Lvc et al.

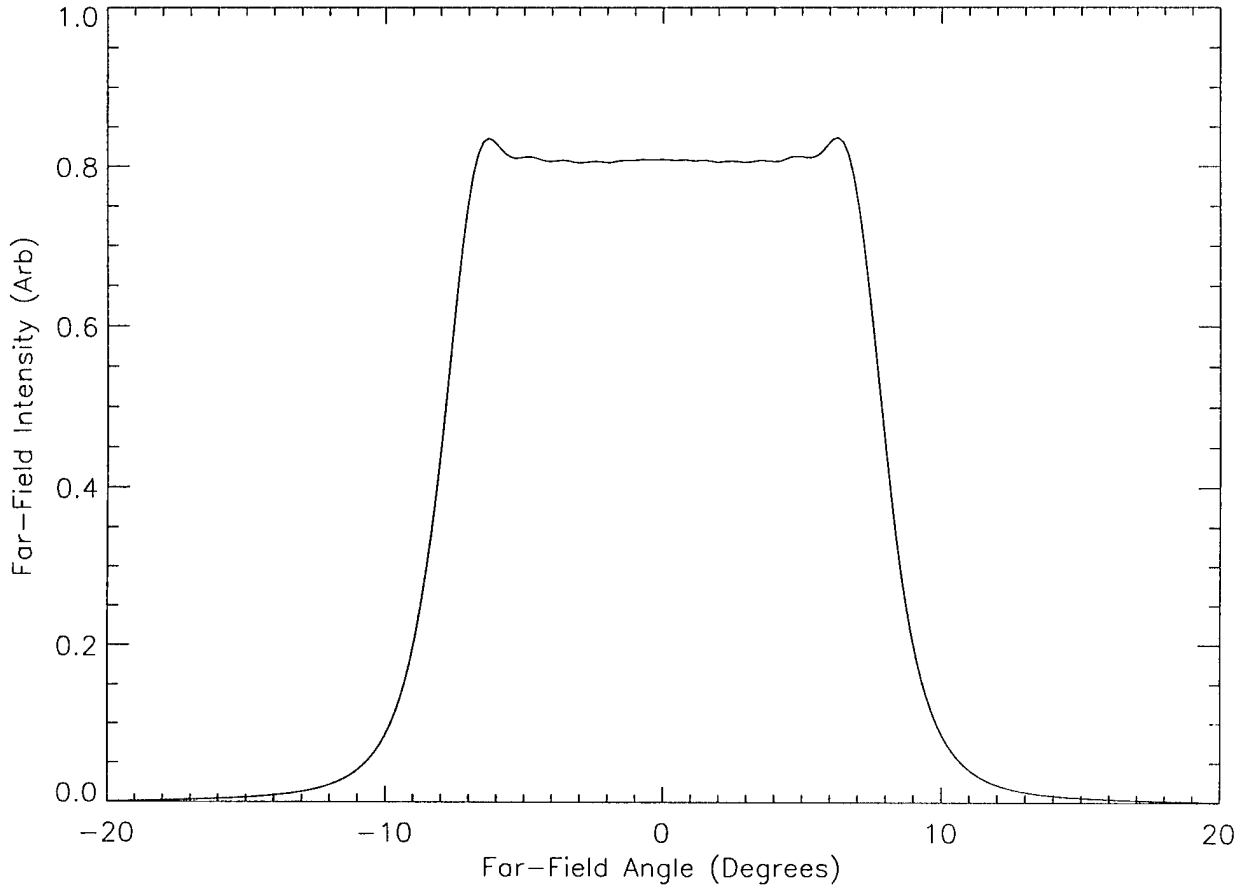
1.0
0.8
0.6
0.4
0.2
0.0
Far-Field Intensity (Arb)
-20
-10
0
10
20
Far-Field Angle (Degrees)

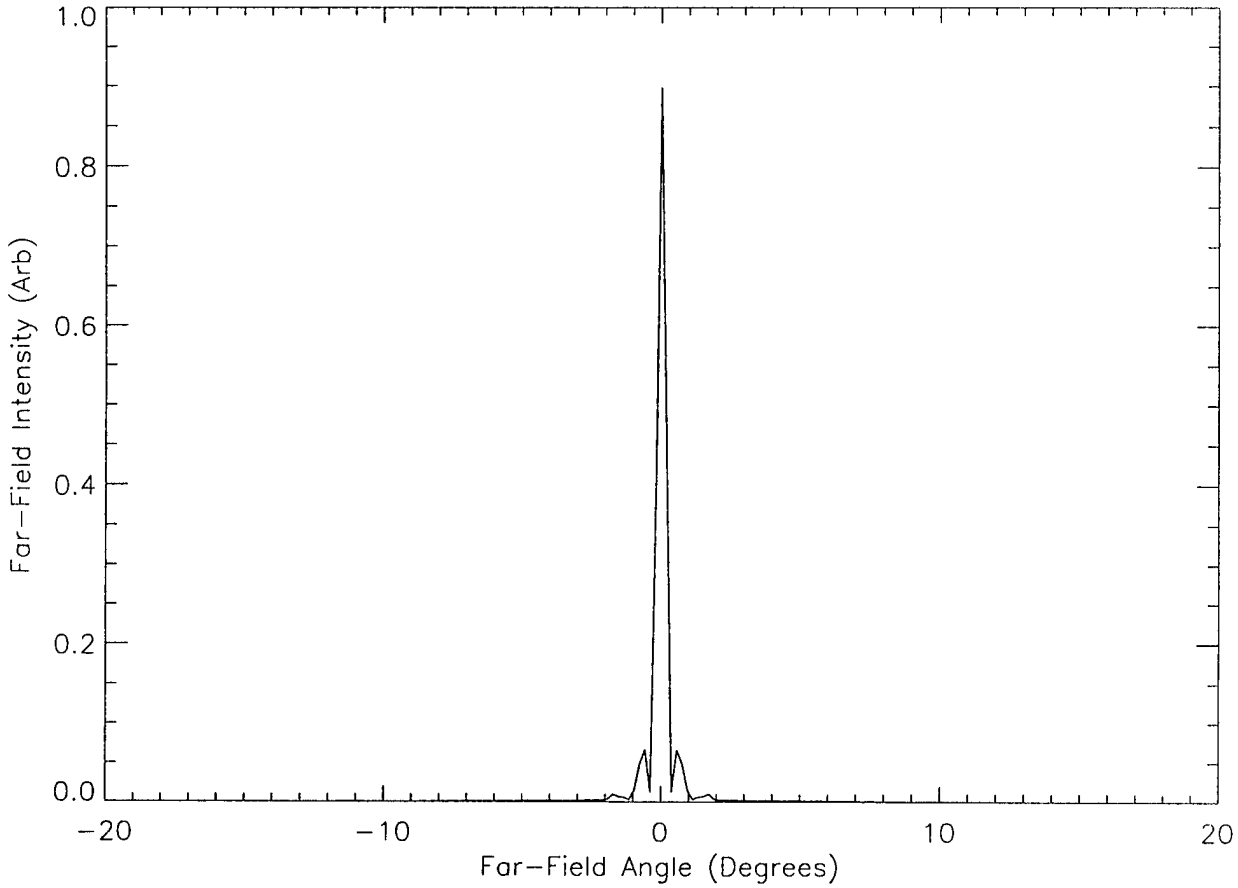
1.0
0.8
0.6
0.4
0.2
0.0
Far-Field Intensity (Arb)
-20
-10
0
10
20
Far-Field Angle (Degrees)

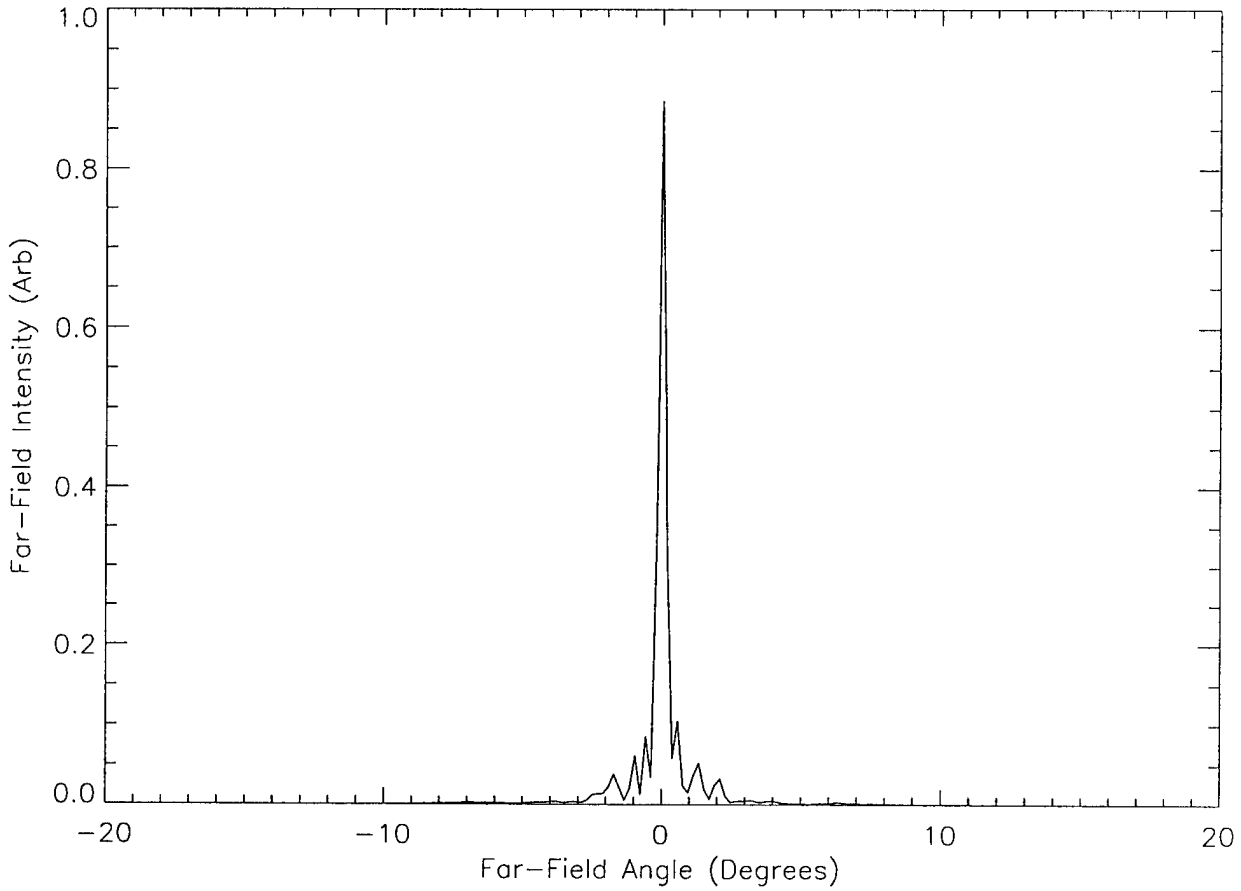
1.0
0.8
0.6
0.4
0.2
0.0
Far-Field Intensity (Arb)
-20
-10
0
10
20
Far-Field Angle (Degrees)

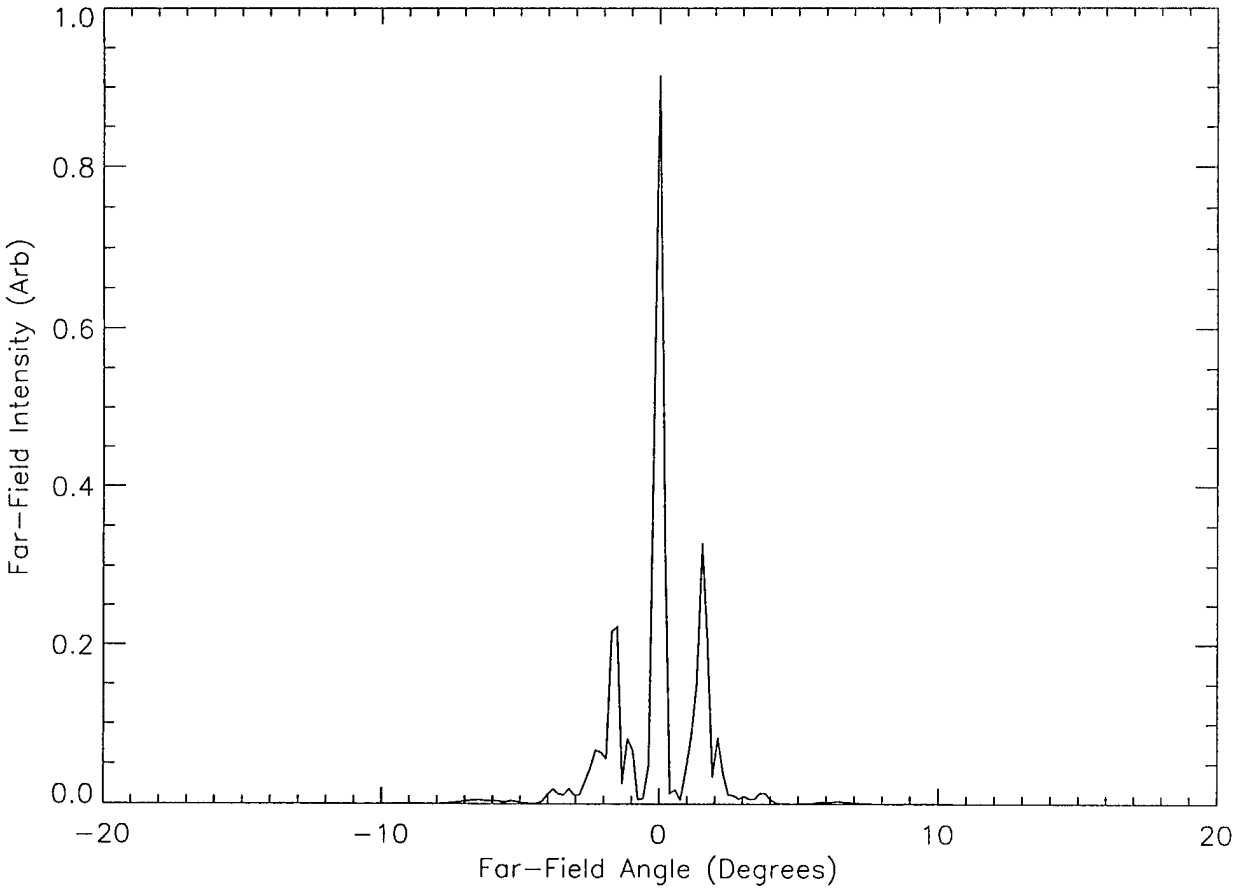

Fig. 5

Lee et al.

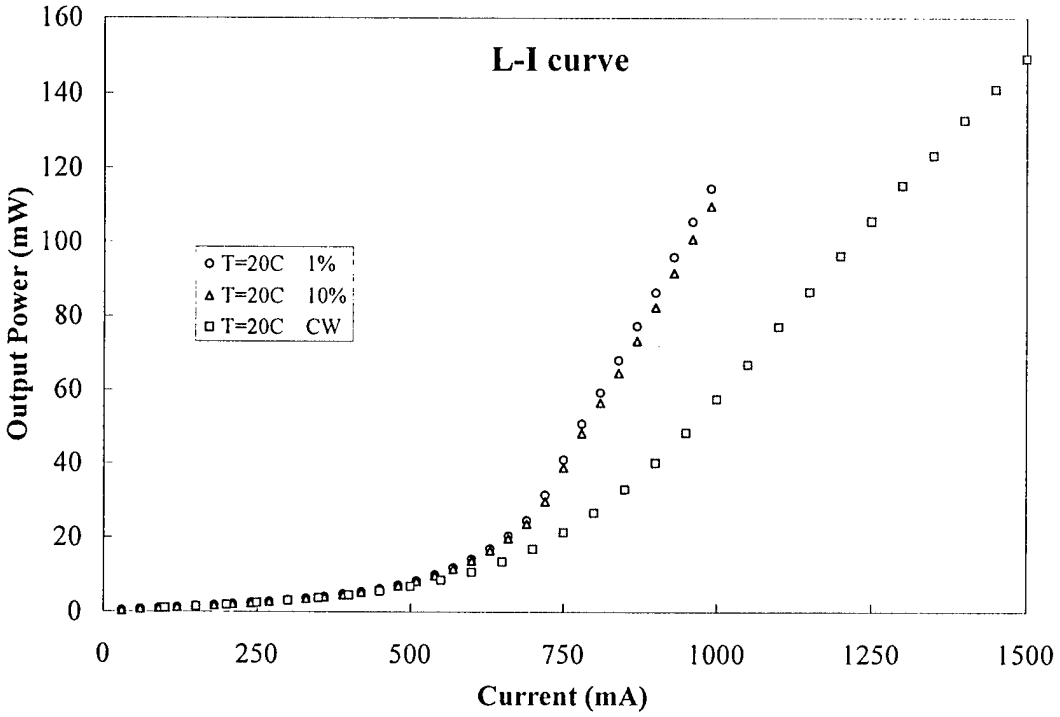

FIG. 6

LLC 03 AL.

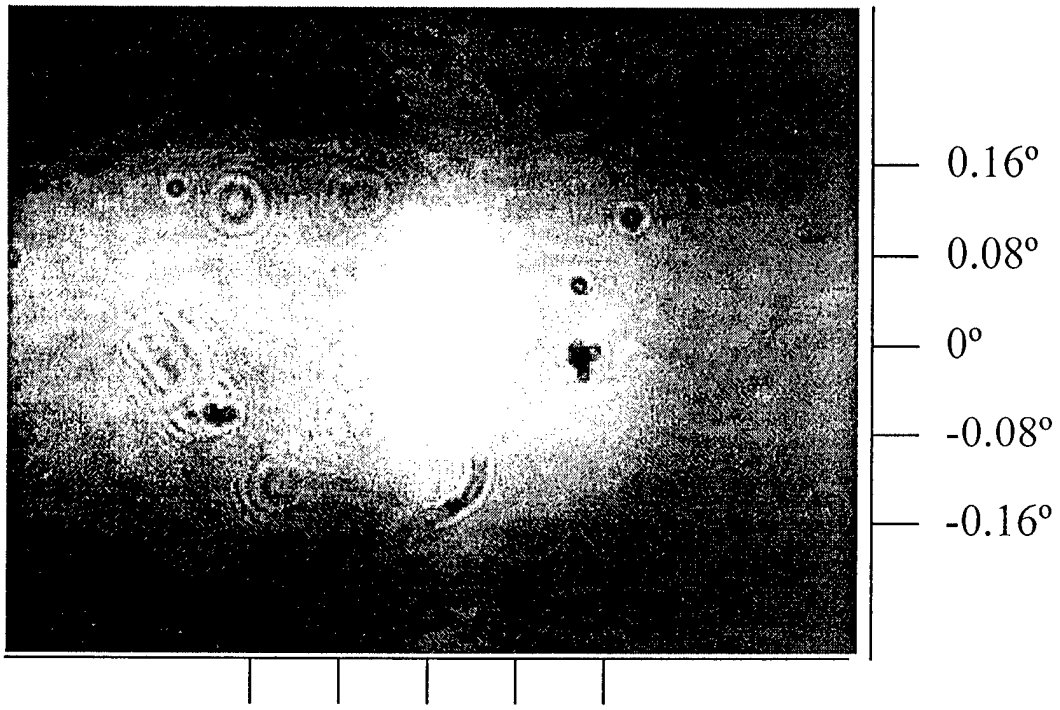

FIG. 7(a)

LEE ET AL.

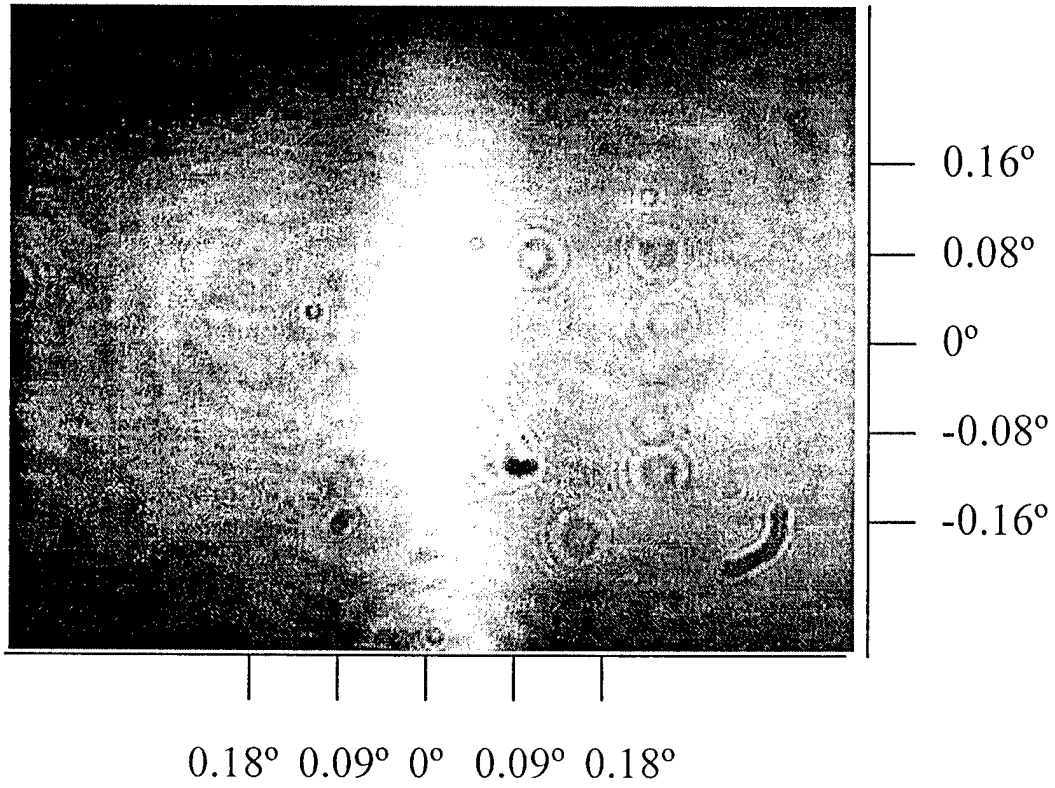

Fig. 7(b)